論 文

Effect of Chemical Composition and Relative Humidity on the Humid Gas Stress Corrosion Cracking of Aluminum Alloys

Aoyama Gakuin University
Takeshi OGAWA
Shota HASUNUMA
Graduate school of Aoyama Gakuin University
Toshiki SHIRAWACHI
Naonari FUKADA

In order to obtain the characteristics of humid gas stress corrosion cracking (HG-SCC), two types of tests have been performed to measure the crack growth rate, da/dt, under load (P)-increasing and displacement (D)-constant conditions for high and low da/dt regions, respectively. The tests are aimed to investigate the effects of chemical composition on the HG-SCC characteristics of standard alloys using specially prepared alloys. The P-increasing test in humid air revealed that da/dt is increased by excess Si content from the balanced composition of Mg_2Si without Cu addition in 6000 series alloys, while by Cu addition, da/dt is reduced and the HG-SCC resistance is improved. The D-constant tests exhibit similar trend of crack growth and small values of the threshold stress intensity factor for HG-SCC, K_{ISCC}, for the excess-Si alloys without Cu. Observations by scanning electron microscope (SEM) demonstrate that the intergranular fracture surface is developed for the alloys having excess Si without Cu, while the dimple fracture surface becomes predominant for the other alloys. HG-SCC characteristics obtained for the standard alloys of 6000 series are consistent with those of the special alloys. 7075 alloy exhibits poor HG-SCC resistance and different crack growth mechanisms as compared with the 6000 series. The results in dry air revealed that da/dt decreased and K_{ISCC} increased remarkably by reducing the humidity for the alloys that have poor HG-SCC resistance. HG-SCC characteristics are independent of plastic pre-strain expected in the autofrettage process.

Keywords : Humid Gas Stress Corrosion Cracking, Chemical Composition, Relative Humidity, Aluminum Alloy, Hydrogen Container

1. Introduction

The hydrogen gas container is one of the most significant components for fuel cell electric vehicles (FCEV). The major types of containers are expected to be made of metal and polymer liners surrounded by carbon fiber reinforced

原稿受付日 18. 5. 30

plastics (CFRP), which are classified as Type 3 and Type 4 containers, respectively. In order to choose an appropriate material for the metal boss and liner, corrosion resistance should be evaluated in humid air environments as well as in the high pressure hydrogen gas for the purpose of commercial vehicle use, since it might be subjected to humid air during service conditions. Presently, acceptable hydrogen gas may contain water vaper below 5 ppm as an impurity for FCEV [1]. When the gas with H_2O of 5 ppm is charged to the container up to 70 MPa at 15℃, the relative humidity, *RH*, increases to be 85 to 90% by decreasing the temperature of −7℃[2]. Therefore, *RH* in the container can be more than 85% in service condition. Depending on the chemical composition of aluminum alloy, it has been discussed a possibility of hydrogen embrittlement due to the following chemical reaction[2].

$$2Al+(3+x)H_2O \rightarrow Al_2O_3 \cdot xH_2O+(3H_2, 6H) \quad (1)$$

It is suspected that the hydrogen element of 6H enters into the material as an atomic hydrogen instead of a gas condition of $3H_2$, and influences on the cracking behavior under static loading condition[2]. This behavior is denoted as humid gas stress corrosion cracking (HG-SCC) and the test method has been standardized by HPIS E 102[3].

Other candidate test method for evaluating the effect of the hydrogen on the HG-SCC is ISO 7866 Annex B. Both in the two standards, precracked specimen is subjected to a static or sustained load for 90 days in air. Judgement is made whether the crack grows a certain distance of 0.16mm or not. This cracking behavior is denoted as a sustained load cracking (SLC) in ISO 7866 Annex B. However, there is no restriction of *RH* in this test method despite the sensitivity of *RH* on the reaction of Eq. (1), while in HPIS E102 *RH* is restricted to be more than 85%. In order to investigate the difference in judgements of HPIS E102 and ISO 7866 Annex B, crack growth characteristics should be clarified in humid and dry air environments in relation to the chemical compositions of aluminum alloys.

The authors have investigated the HG-SCC characteristics of standard alloys of 6061, 6066 and 6351 in the previous works[4),5)]. Similar experiments are performed for 6061 (another lot), 6082 and 7075 in dry air environment as well as in humid air in the present study. In order to investigate the effect of the chemical compositions of the standard alloys on HG-SCC characteristics, special alloys are prepared to have chemical compositions controlled systematically and investigated by the similar experiments performed for the standard alloys. Additional experiments are performed for pre-strained 6061 in order to investigate the influence of autofrettage process.

2. Materials and Experimental Procedures

2.1 Materials and Specimens

Chemical compositions (mass %) of the standard aluminum alloys are presented in Table 1. Alloys of 6061, 6066, 6351, 6082 and 7075 are used in this study. Numbers in parenthesis denote the lot numbers and are consistent with our previous work[5]. FG and CG indicate fine and coarse grains, respectively. Microstructures of 6061(2), 6066(2) and 6351(2) were shown in our previous works[4)~6)]. All the standard alloys tested are subjected to T6 heat treatment, by which the maximum strength is attained. The mechanical properties are presented in Table 2,

where indicator of FG is omitted hereafter.

Tables 3 and 4 show chemical compositions and mechanical properties, respectively, for special alloys prepared for a series of studies supported by the New Energy and Industrial Technology Development Organization (NEDO). The alloys numbered ②, ⑤, ⑧, ⑪ and ⑭ will be used elsewhere. Contents of Si, Mg and Cu are systematically controlled, while those of the other elements are controlled to be as small as possible. The amounts of Mg and Si of the special alloys are plotted in Fig. 1. Since Mg and Si make a binary compound, Mg_2Si, the alloys on the dashed line are denoted as balanced alloys with atomic ratio of Mg/Si of 2, i.e., mass ratio of 1.73. The other alloys are referred to as excess−Si alloys. The Cu content is aimed to be 0% or 1%. All the special alloys tested are subjected to T6 heat treatment.

Also presented in Fig. 1 are ranges of Mg and Si contents for the standard 6000 series alloys.

Specimen geometry is the same as that of our previous work[5]. Single edge notched (SEN) specimens are employed with its width, $W=14$ mm, length, $L=66$mm, and the notch length of 5 mm, where loading and crack growth directions are transverse (T) and longitudinal (L), respectively, i.e. TL orientation. Thickness, B, is 7 mm for the standard alloys and 5 mm for the special alloys. Fatigue precracks are previously introduced with the length of about 1 mm at the notch tip under four point bending (4PB) by the horizontal loading oil hydraulic testing machine (outer span length is 38 mm and inner span length is 58 mm) under the stress intensity factor range, $\Delta K=7\sim10$ MPa$\sqrt{\text{m}}$, at the stress ratio, $R=0.1$, and the cyclic frequency, $f=20$Hz.

Table 1 Chemical compositions of the standard alloys [mass%].

Alloy		Si	Fe	Cu	Mn	Mg	Cr	Zn	Ti
6061	(2)FG,CG	0.6	0.22	0.26	0.01	1.0	0.19	<0.01	0.03
	(3)FG	0.6	0.23	0.25	0.01	0.99	0.19	<0.01	0.03
	(4)FG	0.67	0.18	0.32	0.05	1.1	0.17	0.04	0.03
6066	(1)FG	1.5	0.23	1.0	0.8	1.1	<0.01	<0.01	0.03
	(2)FG,CG	1.5	0.23	1.0	0.8	1.1	<0.01	<0.01	0.03
6351	(1)FG	1.1	0.22	<0.01	0.6	0.6	<0.01	<0.01	0.02
	(2)FG,CG	1.1	0.22	<0.01	0.6	0.6	<0.01	<0.01	0.02
6082	FG	1.0	0.23	<0.01	0.71	0.89	0.14	<0.01	0.03
7075	FG	0.1	0.15	1.6	0.03	2.5	0.19	5.6	0.02

(1)-(4): lot numbers, FG: fine grain, CG: coarse grain

Table 2 Mechanical properties of the standard alloys.

Alloy		Tensile strength (MPa)	Proof stress (MPa)	Elongation (%)
6061	(2)	328	275	19
	(2)CG	304	258	14
	(3)	330	290	18
	(4)	361	333	15
6066	(1)	414	338	15
	(2)	368	299	19
	(2)CG	357	293	19
6351	(1)	334	293	14
	(2)	347	310	12
	(2)CG	322	302	17
6082		353	315	17
7075		591	508	15

Table 3 Chemical compositions of the special alloys [mass%].

Alloy	Si	Fe	Cu	Mn	Mg	Cr	Zn	Ti
①	0.89	0.09	0.01	< 0.01	1.6	< 0.01	0.01	0.01
③	0.93	0.09	1.00	< 0.01	1.6	< 0.01	0.01	0.01
④	0.70	0.10	< 0.01	< 0.01	1.21	< 0.01	< 0.01	0.01
⑥	0.72	0.10	1.05	< 0.01	1.25	0.01	< 0.01	0.01
⑦	1.43	0.10	< 0.01	< 0.01	1.20	< 0.01	< 0.01	0.01
⑨	1.43	0.10	0.98	< 0.01	1.18	< 0.01	< 0.01	0.01
⑩	0.405	0.09	< 0.01	< 0.01	0.71	< 0.01	< 0.01	0.01
⑫	0.421	0.09	1.03	< 0.01	0.73	< 0.01	< 0.01	0.01
⑬	1.105	0.10	< 0.01	< 0.01	0.70	< 0.01	< 0.01	0.01
⑮	1.14	0.10	1.04	< 0.01	0.73	< 0.01	< 0.01	0.01
⑯	1.8	0.11	< 0.01	< 0.01	0.74	< 0.01	0.01	0.01
⑰	1.8	0.11	1.10	< 0.01	0.74	< 0.01	0.01	0.01

Table 4 Mechanical properties of the special alloys.

Alloy	Tensile strength (MPa)	Proof stress (MPa)	Elongation (%)
①	329	313	5.8
③	403	373	7.1
④	315	295	11.5
⑥	408	369	6.9
⑦	371	349	5.3
⑨	401	349	8.3
⑩	273	257	8.4
⑫	362	325	10
⑬	362	331	5.3
⑮	395	334	8.6
⑯	347	321	7.4
⑰	365	326	6.9

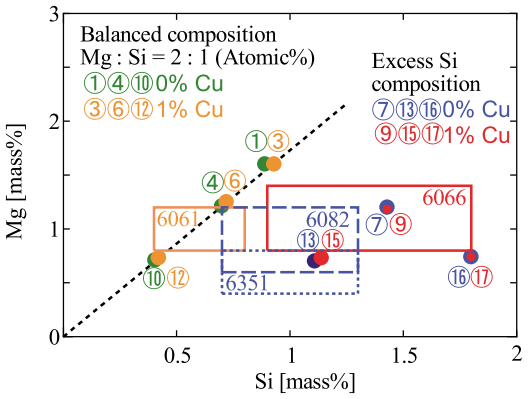

Fig. 1 Contents of main chemical composition of the standard and special alloys.

2.2 Load increasing Test

Method of load (P)−increasing test is the same with that of our previous work[5]. P−increasing tests are carried out in humid air environment (relative humidity, $RH>90\%$), for which the specimens are covered with a plastic bag and an ultrasonic humidifier is used to keep the RH more than 90% without dew. The testing machine was developed in−house using oil hydraulic actuators (HySerpack, Daiichi Denki Co.)[4]. Testing load controlled by personal computer (PC) is applied to the SEN specimens in 4PB. Values of P and the back face strain of the specimens are introduced to the PC and used for the calculation of stress intensity factor, K, where the crack length, a, is determined by unloading elastic compliance method. For this measurement, partial unloading is introduced in the constant load at every 1 ks. It is noted that fatigue crack growth due to this partial unloading is so small as to be ignorable as compared with the growth of HG−SCC. The whole procedure of the P−increasing test is predetermined and carried out by the PC automatically.

2.3 Constant displacement Test

The method of displacement (D)−constant tests is the same with that of our previous study[5]. This test is performed under three point bending (3PB) by a bolt loading, i. e. K−decreasing condition, using the SEN specimen. Based on the clip gage displacement at the mouth of the notch and the precrack length, specific values of the initial K are applied by the bolt loading and the test is continued in a PMMA chamber for 30 days (about 2,600ks). The specimens are kept in humid air ($RH>90\%$) and in dry air, for which the chamber is filled with dry air supplied from a unit which can reduce the dew point of −60℃ (IAC Co., Ltd., P4−QD 10). RH of the dry air is less than 1% at room temperature. After D−constant test, the specimen is broken by fatigue loading in order to determine the HG−SCC growth region. Subsequently, the initially applied K values are corrected by the measurements of precrack length on the fracture surfaces.

3. Results and Discussion

3.1 The Effect of Chemical Composition

Figure 2 presents the variations of a and K for P−increasing tests in humid air for the standard alloys of 6061(3), 6082 and 7075. The HG−SCC behavior begins under a specific K value for each material and the crack continues to grow until fracture. This K value is higher for 6061 than for 6082 and 7075. Figures 3, 4 and 5 demonstrate the fracture surfaces taken with a scanning electron microscope (SEM), near the boundary between the precrack and the HG−SCC region for 6061, 6082 and 7075, respectively. Figures (b) show magnified images of area indicated as rectangles the figures (a). In the HG−SCC region, dim-

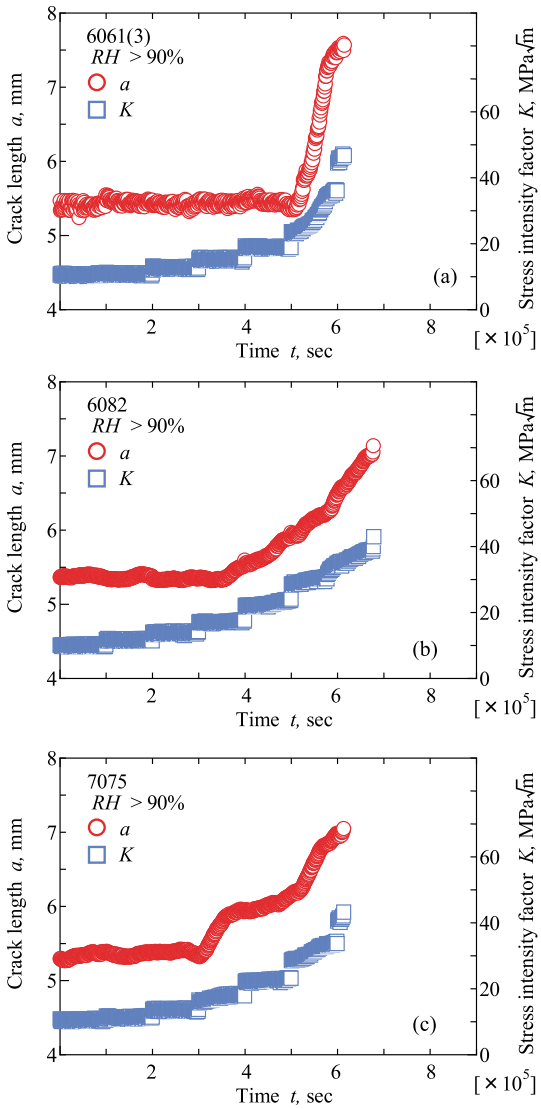

Fig. 2 Variations of a and K under P-increasing tests in humid air for 6061(3)(a), 6082(b) and 7075(c).

ple (transgranular ductile) fracture is predominant for 6061 and 6082, while for 7075 it was difficult to conclude the predominant fracture mechanism although delamination (vertical cracks perpendicular to the macroscopic fracture surface). The delamination implies that intergranular fracture is prone to proceed during HG-SCC since the microstructure of the 7075

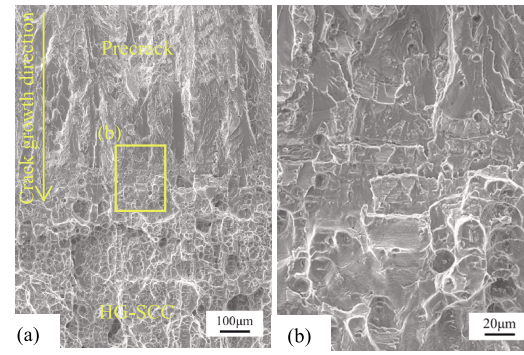

Fig. 3 Fracture surface of 6061(3) alloy obtained by P-increasing test, showing low (a) and high (b) magnification SEM micrographs.

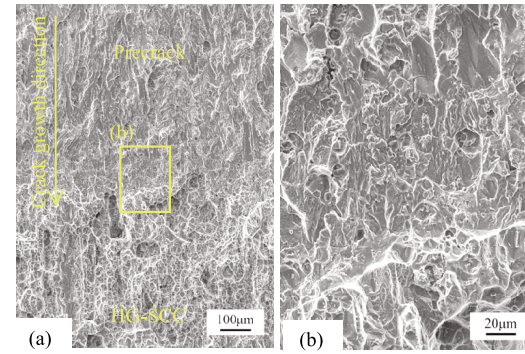

Fig. 4 Fracture surface of 6082 alloy obtained by P-increasing test, showing low (a) and high (b) magnification SEM micrographs.

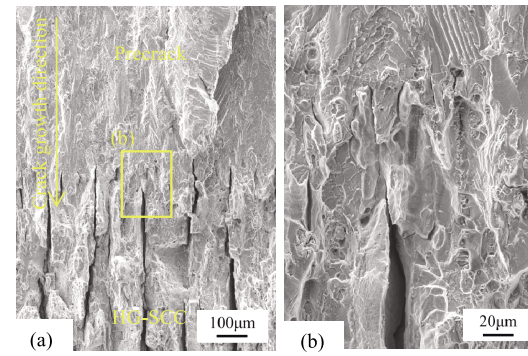

Fig. 5 Fracture surface of 7075 alloy obtained by P-increasing test, showing low (a) and high (b) magnification SEM micrographs.

alloy is expected to consist of pancake structures composed of grains with morphologies thin in thickness direction, extremely and moderately elongated in L and T directions, respectively. Similar morphologies were observed on the specimens tested by the D-constant tests for each alloy.

Figure 6 presents the relationships between crack growth rate, da/dt, and K obtained by the above tests. For the P-increasing tests, the crack growth increment, Δa, values were determined by the compliance method over the constant P conditions as demonstrated in Fig. 2. Since our test system can detect Δa of 0.05mm during the constant load for 100 ks, da/dt of 5×10^{-10} m/s is the minimum to be able to determine. For the D-constant tests, the Δa values were determined in terms of fracture surface observation by averaging 9 point over the thickness. The da/dt is a value of Δa divided by the loading time of 30 days, where the measureable Δa is about 0.01mm by SEM. Thus, the minimum value of the da/dt is 4×10^{-12} m/s by this test. The threshold stress intensity factor for HG-SCC, K_{ISCC}, is determined for this crack growth rate. The data of 6066(1) and 6351(1) were quoted from the tests in Ref. 7, where the test was performed for 90 days, thus the minimum da/dt value should be smaller than the indicated value. Downward arrows indicate that the data are below the minimum values of da/dt. Although some specimens were tested at lower K values than those at the downward arrows, the data plots of these specimens were omitted from the Fig. 6 for clarity.

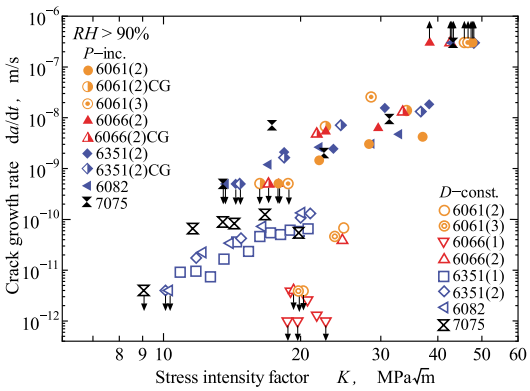

Fig. 6 HG-SCC characteristics of the standard alloys.

In the P-increasing tests, the measurement of da/dt was started at lower K values for 6082, 6351 and 7075 than those for 6061 and 6066 as suggested in Fig. 2. In the subsequent crack growth, there was no apparent trend among the alloys tested until fracture. In the D-constant tests, much lower da/dt values were determined as compared with those in the P-increasing tests. It is notable that K_{ISCC} values are much lower for 6082, 6351 and 7075 than for 6061 and 6066. Therefore, the former group of alloys is susceptible to HG-SCC than the latter.

These HG-SCC tests and fractographic observations were also applied to the special alloys. Figures 7 and 8 demonstrate the SEM micrographs of HG-SCC fracture surface observed just after the introduction of precracks in the P-increasing tests for the alloys without and with Cu, respectively. For the balanced alloys without Cu, i.e., ①, ④ and ⑩, it is observed that typical dimple fracture surface is predominant and the dimple size increase with decreasing contents of Mg and Si. Similar morphology can be observed for the balanced alloys with Cu, i.e., ③, ⑥ and ⑫. On the other hand, intergranular fracture surface can be observed for the excess-Si alloys without Cu, i.e., ⑦, ⑬ and ⑯. This morphology becomes less marked by Cu addition and the dimple fracture is enhanced for the excess-Si alloys with Cu,

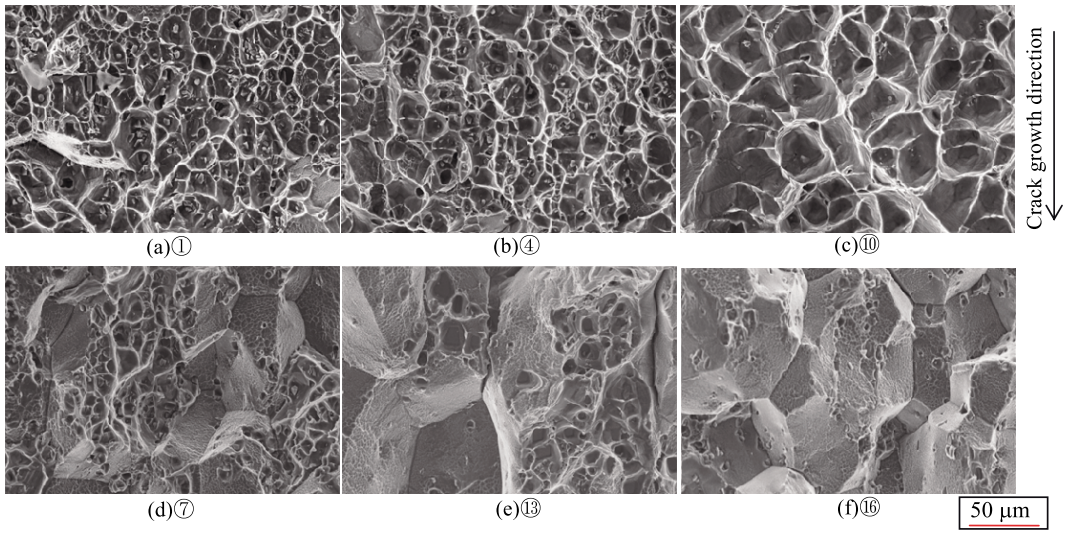

Fig. 7 Fracture surfaces of the special alloys without Cu.

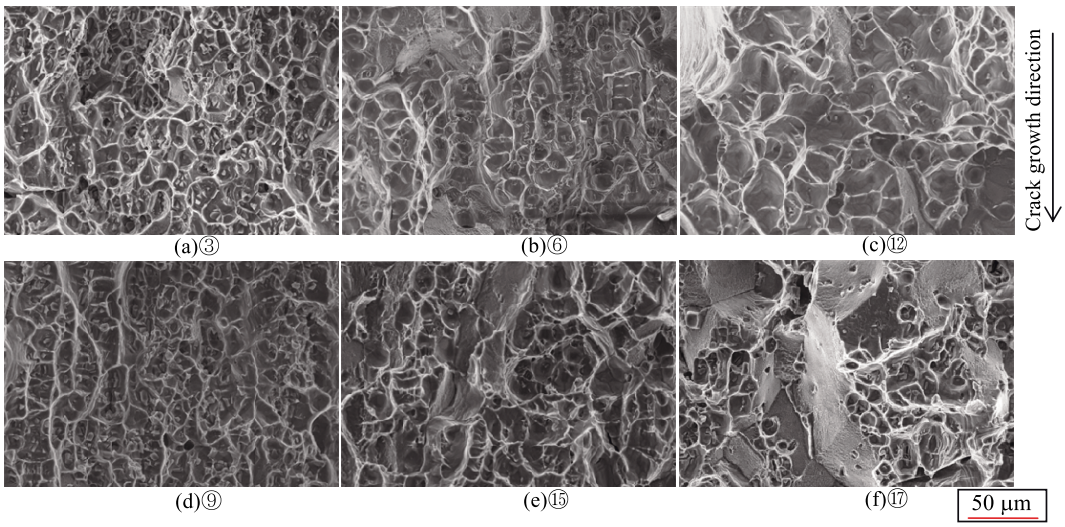

Fig. 8 Fracture surfaces of the special alloys with Cu.

i.e., ⑨, ⑮ and ⑰.

Figure 9 presents the HG-SCC characteristics of the special alloys in terms of the relationships between da/dt and K obtained by the P-increasing and D-constant tests. It is apparent that da/dt at a certain K value and K_{ISCC} values are larger and lower, respectively, for the excess-Si alloys without Cu, i.e., ⑦, ⑬ and ⑯, than those for the other alloys. As shown in Fig. 7, since these materials exhibited intergranular fracture surface, the resistance to HG-SCC was reduced by the change in the crack growth mechanisms (from transgranular to intergranular) of the special alloys. As shown in Fig. 6, 6082 and 6351 exhibited lower resistance to HG-SCC than 6061 and 6066. The formers are excess-Si alloys without Cu, while the latters are either balanced or Cu-containing al-

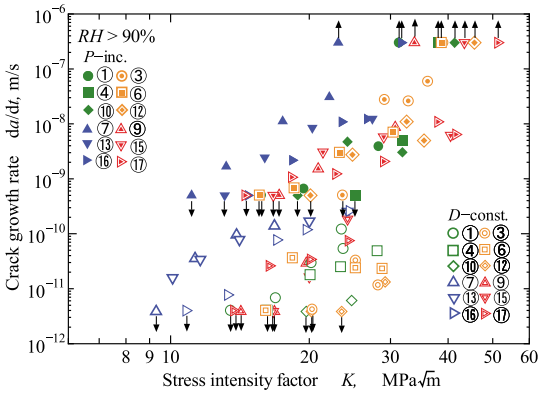

Fig. 9 HG–SCC characteristics of the special alloys.

loys. Therefore, it is confirmed that either Cu addition or balanced composition is effective to improve the resistance to HG–SCC of 6000 series alloys.

3.2 The Effect of Relative Humidity

Figure 10 shows the relationships between da/dt and K obtained by the D–constant tests in humid and dry air environments for the standard alloys of 6061(3), 6082 and 7075 (a), and the special alloys of ⑦, ⑨, ⑩ and ⑫(b). These alloys were selected because of their typical HG–SCC characteristics. The data in humid air were already shown in Figs. 6 and 9. For the alloys of 6082, 7075 and ⑦, crack growth can be observed at much higher K values in dry air than in humid air. The other alloys exhibit similar crack growth characteristics both in humid and dry air environments despite the alloy ⑩ shows a small difference. The former alloys had poor HG–SCC resistance as shown in Figs. 6 and 9. As stated in chapter 1, the difference in judgements between HPIS E 102 and ISO 7866 Annex B is a restriction of *RH* during the tests. The results of Fig. 10 means that the judgment by ISO 7866 Annex B for the alloys having low resistance to HG–SCC will be fluctuated by the humidity. Therefore, restriction of *RH* is necessary as standardized in HPIS E102.

3.3 The Effect of Pre–strain

In the autofrettage process of hydrogen containers, the liner metal is subjected to plastic pre–strain. Therefore, additional D–constant tests were performed in order to investigate the effect of pre–strain on the HG–SCC characteristics. Plate sample of 6061(4) was prepared with the size of 200mm in transverse (T), 75 mm in longitudinal (L) and 7mm in thickness. The plate was plastically elongated in T direction so that the nominal pre–strain of 10.5%

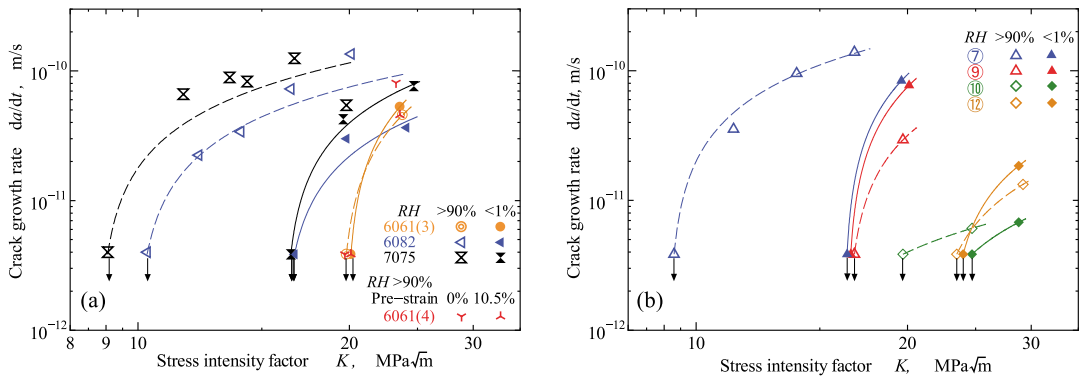

Fig. 10 Comparison of crack growth characteristics obtained by D–constant tests for the standard alloys (a) and the special alloys (b) in humid air (RH > 90%) and dry air (RH < 1%). Also included in (a) is the effect of pre–strain on the HG–SCC characteristics of 6061(4).

was achieved. SEN specimens with $W=14$mm, $L=66$mm and $B=5$mm were cut from the virgin and elongated plate samples in TL orientation. Fig. 10(a) represents the HG-SCC characteristics of 6061(4) with pre-strains of 0 and 10.5% compared with those of 6061(3). The results demonstrate that the HG-SCC characteristics are independent of the pre-strain as well as the lot number.

4. Conclusions

In order to evaluate HG-SCC characteristics, two types of tests have been performed for standard and special alloys. The results obtained are summarized as follows.

(1) For the special alloys, the load-increasing test in humid air revealed that da/dt is increased by excess Si content from the balanced composition of Mg_2Si with no Cu addition, while by Cu addition, da/dt is reduced and the HG-SCC characteristics are improved. The constant-displacement tests exhibit similar trend of crack growth and small values of the threshold stress intensity factor for HG-SCC, K_{ISCC}, for the excess-Si alloys without Cu addition.

(2) Observations by scanning electron microscope (SEM) demonstrate that the intergranular fracture surface is developed for the alloys having excess Si without Cu, while the dimple fracture surface becomes predominant for the other alloys.

(3) HG-SCC characteristics obtained for the standard alloys of 6000 series are consistent with those of the special alloys. 7075 alloy exhibits poor HG-SCC resistance and different crack growth mechanisms as compared with the 6000 series.

(4) For the selected alloys, the results in dry air revealed that da/dt decreased and K_{ISCC} increased remarkably by reducing the humidity for the alloys that have poor HG-SCC resistance.

(5) HG-SCC characteristics are independent of plastic pre-strain expected in the autofrettage process.

Acknowledgement

A part of this work was supported by the New Energy and Industrial Technology Development Organization (NEDO) as a re-commissioned research from Japan Automobile Research Institute. We would like to express our gratitude to the persons concerned.

References

1) ISO 14867-2：2012 Hydrogen fuel-Product specification-Part 2：Proton exchange membrane (PEM) fuel cell applications for load vehicles.
2) Ito, G.；“Service Environment and Testing Method for Global Standardization of Aluminum Alloys Related to Hydrogen”, Corrosion Engineering, Vol. 65, pp. 339-346 (2016). (ISSN 0892-4228)
3) HPIS E 103：2018, Standard Test Method for Humid Gas Stress Corrosion Cracking of Aluminium Alloys for Compressed Hydrogen Containers (2018).
4) Ogawa, T., Hasunuma, S., Sogawa, N., Yoshida, D., Kanezaki, T. and Mano, S.；“Characteristics of Fatigue Crack Growth and Stress Corrosion Cracking in Aggressive Environments of Aluminum Alloys for Hydrogen Gas Containers”, ASME 2014 Pressure Vessels & Piping Conference CD-ROM, PVP2014-28236. pdf, p. 10 (2014).
5) Ogawa, T., Hasunuma, S., Watanabe, S., Sogawa, N., Kanezaki, T., Mano, S. and Miyagawa, K.；“Study on Evaluation Methods for Stress Corrosion Cracking and Fatigue Crack Growth of Aluminum Alloys for Hydrogen Containers”, Journal of High Pressure Institute of Japan, Vol. 54, Issue 6, pp. 277-288 (2016).
6) Ogawa, T., Sugiyama, Y., Kanezaki, T. and Hayashi, N.；“Characteristics of Corrosion Fatigue Crack Growth in Salt Water of Aluminum Alloys for Hydrogen Gas Containers”, ASME 2013 Pressure Vessels & Piping Conference CD-ROM,

PVP2013-97259.pdf, p.9（2013）.
7）Kanezaki, T., Mano, S., Miyagawa, K., Hayashi, N. and Ogawa, T. ; “Life Design and Evaluation Method of Type 3 High-Pressure Hydrogen Tank for Fuel Cell Electric Vehicle”, Honda R&D Technical Review, Honda R&D Co., Ltd, Vol.24, No.1, pp.150－159（2014）.

【著者紹介】
小川 武史（Takeshi OGAWA）
青山学院大学
College of Science and Engineering, Aoyama Gakuin University, 5－10－1, Fuchinobe, Chuou－ku, Sagamihara, Kanagawa, 252－5258, Japan
TEL : 042－759－6203 FAX : 042－759－6502
E－mail : ogawa@me.aoyama.ac.jp

蓮沼 将太（Shota HASUNUMA）
青山学院大学
College of Science and Engineering, Aoyama Gakuin University, 5－10－1, Fuchinobe, Chuou－ku, Sagamihara, Kanagawa, 252－5258, Japan
TEL : 042－759－6210 FAX : 042－759－6502
E－mail : hasunuma@me.aoyama.ac.jp

白輪地 峻輝（Toshiki SHIRAWACHI）
青山学院大学大学院
College of Science and Engineering, Aoyama Gakuin University, 5－10－1, Fuchinobe, Chuou－ku, Sagamihara, Kanagawa, 252－5258, Japan
FAX : 042－759－6502
E－mail : c5617119@aoyama.jp

深田 直也（Naonari FUKADA）
青山学院大学大学院
College of Science and Engineering, Aoyama Gakuin University, 5－10－1, Fuchinobe, Chuou－ku, Sagamihara, Kanagawa, 252－5258, Japan
FAX : 042－759－6502
E－mail : c5618150@aoyama.jp